Atmos. Meas. Tech. Discuss., 8, 7201–7237, 2015
www.atmos-meas-tech-discuss.net/8/7201/2015/
doi:10.5194/amtd-8-7201-2015
© Author(s) 2015. CC Attribution 3.0 License.

Atmospheric Measurement Techniques Discussions
Open Access

This discussion paper is/has been under review for the journal Atmospheric Measurement Techniques (AMT). Please refer to the corresponding final paper in AMT if available.

Characterization of Mediterranean hail-bearing storms using an operational polarimetric X-band radar

G. Vulpiani[1], L. Baldini[2], and N. Roberto[2]

[1]Department of Civil Protection, Rome, Italy
[2]Institute of Atmospheric and Climate Sciences – National Research Center, Rome, Italy

Received: 12 June 2015 – Accepted: 18 June 2015 – Published: 14 July 2015

Correspondence to: G. Vulpiani (gianfranco.vulpiani@protezionecivile.it)

Published by Copernicus Publications on behalf of the European Geosciences Union.

Abstract

This work documents the fruitul use of X-band radar observations for the monitoring of severe storms in an operational framework. More specifically, a couple of severe hail-bearing Mediterranean storms occurred in 2013 in southern Italy, flooding two important cities of Sicily, are described in terms of their polarimetric radar signatures and retrieved rainfall fields. It is used the X-band dual-polarization radar operating inside the Catania airport (Sicily, Italy), managed by the Italian Department of Civil Protection. A suitable processing is applied to X-band radar measurements. The crucial procedural step relies on the differential phase processing based on an iterative approach that uses a very short-length (1 km) moving window allowing to properly catch the observed high radial gradients of the differential phase. The parameterization of the attenuation correction algorithm, which use the reconstructed differential phase shift, is derived from electromagnetic simulations based on 3 years of DSD observations collected in Rome (Italy). A Fuzzy Logic hydrometeor classification algorithm was also adopted to support the analysis of the storm characteristics. The precipitation fields amount were reconstructed using a combined polarimetric rainfall algorithm based on reflectivity and specific differential phase. The first considered storm was observed on the 21 February, when a winter convective system, originated in the Tyrrhenian sea, hit only marginally the central-eastern coastline of Sicily causing the flash-flood of Catania. Due to the optimal radar location (the system is located at just few kilometers from the city center), it was possible to well retrieve the storm characteristics, including the amount of rainfall field at ground. Extemporaneous signal extinction, caused by close-range hail core causing significant differential phase shift in very short range path, is documented. The second storm, occurred on 21 August 2013, is a summer mesoscale convective system originated by the temperature gradient between sea and land surface, lasted a few hours and eventually flooded the city of Siracusa. The undergoing physical process, including the storm dynamics, is inferred by analysing the vertical sections of the polarimetric radar measurements. The high registered precipitation amount was fairly

CC BY

well reconstructed even though with a trend to underestimation at increasing distances. Several episodes of signal extinction clearly manifested during the mature stage of the observed supercell.

1 Introduction

Dual-polarization technology has greatly improved the quality of radar precipitation measurements and have reduced the gap between the qualitative and quantitative use of radar observations. Several operational S- and C-band radar networks have been (or will be soon) upgraded to adopt dual-polarization technology. In the last decade many studies have been undertaken to explore the benefit of polarimetry for Quantitative Precipitation Estimation (QPE) using X-band radars (Anagnostou et al., 2004; Matrosov et al., 2005; Wang and Chandrasekar, 2010; Anagnostou et al., 2010; Matrosov et al., 2013), which are de facto very appealing systems due to their compact size, transportability and, generally, affordable cost. In the presence of hail or melting hail, QPE algorithms based on differential phase shift are a convenient mean to estimate the fraction of liquid phase precipitation (Matrosov et al., 2013; Ryzhkov et al., 2013). Notwithstanding, in spite of effectiveness and robustness of correction methods based on dual-polarization measurements and the performance of rainfall algorithms based on specific differential phase shift, which are immune to attenuation, the latter remains the major impairment for the operational use of X-band systems. In the presence of heavy rain and hail mixture, partial attenuation can be further enhanced up, turning to return extinction. Heavy rain above the radar can wet the radome adding further attenuation (see Bechini et al., 2010 and Schneebeli et al., 2012 for measurements collected by the same radar used in this paper). Moreover, some applications, such as the discrimination of between rain and hail radar echoes requires the use of attenuation corrected reflectivity and differential reflectivity. If objective of radar observation includes the analysis of internal structure of hail-bearing convective cells to forecast their degree of severity and their evolution in time, differential phase measure-

AMTD
8, 7201–7237, 2015

CC BY

ments are not sufficient. Discrimination between rain and hail using radar returns is a long-standing objective of radar meteorology with impact on nowcasting, rainfall estimation assessment, microphysical investigation, aviation, and agricultural applications. Hail detection, using single-polarization radar, began in the late 1950s with techniques based on reflectivity measurements considering the echo intensity, its structure, and their time evolution during the hailstorm (Cook, 1958; Douglas and Hitschfeld, 1958). Mason (1971) suggested a 55 dBZ reflectivity threshold as an indicator of the presence of hail in S-band radars. A refinement of the relationship between the 45 dBZ level above the freezing layer and the occurrence of hail at ground (Waldvogel et al., 1979) is currently used by the Weather Surveillance Radar-1988 Doppler (WSR-88D) single polarization systems. Dual-wavelength methodologies making use of the ratio of reflectivities measured at S- and X-bands were also proposed (Atlas and Ludlam, 1961; Eccles and Atlas, 1973). However, with the development of radar dual-polarization techniques, (Seliga and Bringi, 1976) the differential reflectivity Z_{DR} became the key radar measurement for hail detection (Seliga et al., 1982; Aydin et al., 1984, 1986; Bringi et al., 1984). The common underlying hypothesis of dual-polarization methods is the isotropic radar appearance of hail even if it is oblate: tumbling and gyrating motions confer a spherical-like behavior to hail (Knight and Knight, 1970) that make the corresponding Z_{DR} signature being near to zero. Based on disdrometer observations, Aydin et al. (1986) suggested identifying hail by measuring the departure of observed reflectivity factor and differential reflectivity from an empirically derived hail-rain boundary. Moreover, Zrnić et al. (1993) the authors assumed that large hail, independently from the initial orientation (either oblate or prolate hailstones), tends to fall vertically producing negative values of Z_{DR}. Observations of hailstones with the major axis in the horizontal are also documented in the literature (Smyth et al., 1999). According to the model proposed by Rasmussen and Heymsfield (1987), the water coat surrounding melting hail tends to stabilize the major axis in the horizontal direction, as it was proved by Tabary et al. (2009) using C-band radar observations. Consequently, the fall mode, determined by the Liquid Water Content (LWC) and updraft speed, is a crucial factor

CC BY

affecting the interpretation of polarimetric radar signatures and the development of hail detection algorithms. Validation studies have confirmed the higher performance of dual-polarization hail detection algorithms with respect to methodologies employing radar reflectivity only for the diagnosis of hail using radar measurements at S-band Heinselman and Ryzhkov (2006). The set of measurements provided by a dual-polarization radar, namely reflectivity factor at horizontal polarization (Z_H), differential reflectivity (Z_{DR}), differential propagation phase shift (Φ_{DP}), from which the specific differential phase (K_{DP}), is calculated, the copolar correlation coefficient (ρ_{HV}) and, when available, the linear linear depolarization ratio (L_{DR}), was exploited, starting from the late 1990s, in fuzzy logic hydrometeor classification systems, initially proposed for S-band radar (Vivekanandan et al., 1999; Liu and Chandrasekar, 2000; Zrnić et al., 2001). Investigations involving the above mentioned set aimed also at identifying characteristics of hail-bearing precipitation cells that can be used by forecaster to infer the severity and future evolution of the storm. The most known of these features is referred to as "Z_{DR} column" that is the appearance of positive differential reflectivity above the 0° isothermal from which information be related to location and strength of updraft can be inferred (Illingworth et al., 1987; Kumjian et al., 2014 and references therein). However, such studies have shown that not only Z_{DR}, but other dual-polarization variables should be used to correctly interpret behaviour of convective cells. At attenuating frequencies and particularly at X-band, identification of hail and investigation of hail-bearing cells is more difficult. In particular, differential attenuation might have detrimental effects on any methodology involving differential reflectivity, since effects of attenuation, or even effects of wrong attenuation correction, can mask intrinsic polarimetric signatures. In the present work, some characteristics of the examined storms are in fact explained by looking at the perturbation of the polarimetric radar signatures (e.g., enhanced attenuation, prominent depression of the copolar correlation coefficient). Due to the recent success of dual-polarization X-band systems, case studies related to heavy precipitation, involving hail or hail mixed with rain, have been reported in the literature (Matrosov et al., 2013; Figueras and Ventura et al., 2013; Snyder et al., 2010). Notwithstanding,

AMTD
8, 7201–7237, 2015

basic ingredients for identifying graupel and hail formation within a convective cell can be obtained by the comparative analysis of the polarimetric radar observations. The applied Fuzzy Logic hydrometeor classification scheme is only used in this paper as additional analysis support system. The manuscript is organized as follows: Sect. 2 describes the operational contest and the data processing methodology, the considered precipitation events are deeply analyzed in Sect. 3.

2 Radar and data processing systems

2.1 Operational scenario

The SELEX-Gematronik 50 DX polarimetric system with a 3 dB beam width of 1.3° and 50 kW of transmit peak power was considered in this work. It was deployed at the airport of Catania (Sicily) by the end of 2010 and is currently integrated as gap filler within the national weather radar network, either for weather or volcanic ash cloud monitoring (Marzano et al., 2013). The operational volume observation strategy, repeated every 10 min, includes 12 PPI sweeps, with antenna elevation angle ranging from 1 to 21.6°, and a vertical-incidence scan used for Z_{DR} calibration and for a detailed characterization of the column above the radar. The adopted PRF is 1875 Hz, which corresponds to a maximum unambiguous range of 80 km, while the range resolution is 200 m. Due to the presence of the Etna volcano, whose peak (about 3.2 km a.s.l.) is located at about 30 km north from the radar, a wide azimuth sector (about 90°) is shielded at low elevation scans, as depicted in Fig. 1. At 3°, the shielded sector shrinks to about 20° of width, becoming almost negligible at 5°.

2.2 Processing methodology

The main steps of the applied processing chain, i.e., differential phase processing, attenuation correction and rainfall estimation, are here shortly summarized. Further details can be found in Vulpiani et al. (2012).

AMTD
8, 7201–7237, 2015

CC BY

a. *Differential reflectivity calibration*. Z_{DR} is calibrated through vertical scan observations resorting to the hydrometeors properties (Gorgucci et al., 1999).

b. *Ground clutter identification*. A Fuzzy-Logic based approach resorting to the concept of data quality is applied (Vulpiani et al., 2012).

c. *Specific differential phase retrieval*. The iterative moving-window range derivative scheme proposed by Vulpiani et al. (2012) is applied in the present work. It can be summarized through the following few steps:

   i. K_{dp} retrieval (first guess). A first guess of the specific differential phase (K'_{dp}) is retrieved from the raw differential phase through a finite-difference scheme over a given sized moving window.

   ii. K_{dp} check. The out-of-range K_{dp} values are nullified.

   iii. Φ_{dp} reconstruction. The filtered differential phase is estimated as $\Phi_{dp}(r) = 2\int_0^r K_{dp}(s)\mathrm{d}s$

   iv. K_{dp} retrieval (final guess). The final estimation of the specific differential phase K_{dp} is then obtained as range derivative of the reconstructed Φ_{dp}.

Steps (iii)–(iv) are repeated iteratively to reduce the expected K_{DP} standard deviation $\sigma_{K_{DP}}$. Indeed, according to the uncertainty propagation theory, the standard deviation of the final K_{DP} can be expressed (Vulpiani et al., 2012) as

$$\sigma(K_{dp}) = \frac{1}{\sqrt{2N}} \frac{\sigma(\Psi_{dp})}{L} \tag{1}$$

where N is the number of range gates contained in the L sized moving window (i.e., $N = L/\Delta r$, Δr being the range resolution).

It is worth mentioning that the retrieved differential phase is not affected by the system offset, it being removed through the derivative computation. This feature

AMTD
8, 7201–7237, 2015

CC BY

is particularly useful for attenetuation correction purposes based on differential phase shift measurements.

In advance with respect to the description of considered precipitation events, Fig. 2 shows, as example, the raw and reconstructed differential phase profiles observed on the 21 August 2013 at 04:50 UTC. The a-posteriori estimated offset has been added to the filtered Φ_{DP} for easier comparison. It is worth noting that the length of the adopted moving window (1 km), shorter with respect to that used in other Φ_{DP} filtering scheme (e.g. Figueras and Ventura et al., 2013) allows to catch small-scale phase gradients (thus avoiding an excessive smoothing of rainfall fields) whereas, at the same time, the iterative scheme enables to smooth noise effects.

d. *Attenuation correction*. The common polarimetric approach for compensating rain path attenuation is based on the assumed linearity between specific attenuation, as well as differential attenuation, and specific differential phase (Bringi et al., 1990, 2001; Carey et al., 2000; Testud et al., 2000), i.e. $A_{H,DP} = \gamma_{H,DP} K_{DP}$.

   The parameterization adopted in the present work was obtained from T-Matrix scattering simulations based on the three years of DSD observations collected in Italy (Adirosi et al., 2015), i.e., $\gamma_H = 0.29$, $\gamma_H = 0.048$.

e. *Rainfall estimation*. The polarimetric rainfall algorithm proposed by Vulpiani and Baldini (2013), based on the use of reflectivity factor and specific differential phase, is applied in the present study. With the aim to gradually use R_K at increasing rainfall regimes, the combined algorithm takes the form of a weighted sum

$$R_C = w_K \cdot R_K + (1 - w_K) \cdot R_Z \quad (2)$$

where R_Z and R_K are the rainfall estimates obtained applying specific power laws to the lowest beam map of Z and K_{DP}, respectively. The R–K parameterization is

AMTD
8, 7201–7237, 2015

Characterization of Mediterranean hail-bearing storms

G. Vulpiani et al.

CC BY

based on the study carried out by Adirosi et al. (2015) ($R = 14.69K_{DP}^{0.84}$), whereas the Marshall and Palmer (1948) coefficients are adopted to derive R_Z.

The weight w_K is defined as

$$w_K = \begin{cases} 0, & \text{if } K_{dp} \leq 0.5 \\ 2 \cdot K_{dp} - 1, & \text{if } 0.5 < K_{dp} < 1 \\ 1, & \text{if } K_{dp} \geq 1 \end{cases} \tag{3}$$

f. *Hydrometeor classification*. The applied hydrometeor classification approach is based on the fuzzy logic scheme proposed by Liu and Chandrasekar (2000), adapted for X-band following Dolan and Rutledge (2009), which input parameters are the polarimetric radar observables (Z_H, Z_{DR}, K_{DP}, ρ_{HV}) and the height of the melting layer. The algorithm attempts to identify the following six hydrometeor types: rain (a unique class for all type of liquid hydrometeor), wet snow, dry snow, graupel and small hail, hail and rain–hail mixture.

3 Storm analysis

3.1 21 February 2013 case study

The first considered precipitation event was observed on the 21 February 2013. It was a winter convective system that hit only marginally Sicily causing the flash flood of Catania located on the central-eastern coastline. Fortunatley, most of the precipitation fell over sea. According to press reports, hail was also observed. Looking at the brightness temperature images at µm shown on Fig. 3, it can be noticed that around 15:00 UTC a cold system (cloud top less than 220 K) approched the Sicilian eastern coast where it lasted about 3 h. The lower left panel also shows the intense ligthning observed by the LAMPINET network (Biron, 2009) between 15:00 and 18:00 UTC, confirming the convective nature of the storm. Figure 4 shows the azimuth-average vertical profiles of Z, Z_{DR}, ρ_{HV} and V, as observed at vertical incidence at 16:50 UTC, when the stratiform tail of the storm overpassed the radar site. Such profiles suggest that height of the 0° isothermal is 2100 m above radar. Focusing on the differential reflectivity profile below the melting or in the snow region, a negligible calibration bias can be noticed. The minimum of ρ_{HV} is found below the reflectivity maximum, where the hydrometeor population becomes most heterogeneous. With reference to Fig. 5, showing some frames of the Vertical Maximum Intensity (VMI), it might be noticed that around 15:00 UTC the storm was characterized by a localized intense core in the proximity of the radar site with reflectivity values exceeding 60 dBZ. Whereas the rest of the radar image shows light to moderate values of reflectivity. A northward shielded sector, originated by signal extinction, is quite evident on the tail of the convective core. At 16:00 UTC, the VMI image shows lower reflectivity values, likely related to wet-radome effects originated by the storm core located approximately above the radar site. The precipitation nucleus moved south-eastern leaving the city of Catania around 17:00 UTC. Focusing on the shielded azimuthal sector which manifested at 15:00 UTC, Fig. 6 shows the pseudo-RHIs of the radar observables at 5° of azimuth. Two intense precipitaion cores are evident from the reflectivity slice, respectively located at about 5 and 8 km from the radar site. They are responsible for the signal extinction which is mainly affected the lower tilts. The second reflectivity core exceeds the presumed freezing layer height by 1 km, at least, prefiguring the presence of an hail nucleus. Despite the adopted scan inhibits the sampling above about 1.8 km a.s.l. at short range distances, similar behaviour can be argued for the first core by resorting to physical continuity. Within the first reflectivity nucleus, high values of differential reflectivity are found below 1 km a.s.l. The corresponding values of K_{DP} (up to 6 ° km^{-1}) and ρ_{HV} (mostly below 0.95) might be congruent with the coexistence of rain and hail precipitation. Within the second convective core, values of Z_{DR} larger than 1 dB are found also above the 0° isothermal, topped by low values of ρ_{HV}, likely related to supercooled water drops. At altitudes lower than the presumed melting layer base, the noticeable decrease of ρ_{HV} can be referred to

AMTD
8, 7201–7237, 2015

CC BY

rain and hail mixture with high water fraction as inferable by the corresponding values of K_{DP} and confirmed by the results of the classification algorithm. Figure 7, showing the range plots at 6° of antenna elevation for the same azimuth, points out the effects of attenuation. The swiftly decrease of Z, reaching the Minimum Detectable Z (MDZ) at about 13 km from the radar, where the phase shift exceded 130° in just 8-km path, culminated with total extinction. It is worth noting the factitious asymptotic behaviour of measured Z_{DR} which dropped down to the bottom scale (−5 dB) due to attenuation. Finally, Fig. 8 shows the map of precipitation cumulated in 3 h, as retrieved by the combined polarimetric algorithm described by Eq. (2). The precipitation peak observed on land areas is very close to the radar site. The rain gauge located in Catania registered about 60 mm in 1 h (from 15:00 to 16:00 UTC) and about 70 mm in 1 h and half, the other available gauges registered less than 20 mm in 3 h. The accuracy of the combined rainfall algorithm R_C has been evaluated in terms of mean error $\langle \varepsilon \rangle = \langle R_R - R_G \rangle$, error standard deviation $\sigma = \langle (R_R - R_G)^2 \rangle^{1/2}$, RMSE = $\sqrt{(\langle \varepsilon^2 + \sigma^2 \rangle)}$, FSE = RMSE$/\langle R_G \rangle$, and BIAS = $\langle R_R \rangle / \langle R_G \rangle$. The angle brackets denote the average operator, whereas R_R and R_G refer to the radar estimate and gauge observation, respectively. The results, summarized in Table 1, point out the improvement obtained by the combined polarimetric technique in terms of RMSE, FSE and BIAS if compared with the conventional Z–R relationship. It is worth mentioning that R_K slightly outperforms R_C in terms of BIAS whereas the RMSE is higher because of the error standard deviation.

3.2 21 August 2013 case study

The strong temperature gradient between sea and land surface originated the severe the mesoscale convective system that hit Sicily on the 21 August 2013. The resulting intense precipitation flooded several towns of the estearn coast, including Siracusa. The system originated around 04:00 UTC, lasted about 6 h. The maximum precipitation amount, registered in just two hours by the rain gauge located in Siracusa, exceeded 180 mm, whereof 135 mm observed in just 1 h. Even in this case, most of precipita-

CC BY

tion fell over the sea and hail was also reported at ground. Figure 9 shows some time frames of the brightness temperature at 10.8 µm as retrieved by MSG. The embryo of the convective cloud formed around 04:00 UTC over the Ionian sea. After 1 h two main convective systems are clearly identifiable before they get merged around 06:00 UTC producing the maximum effects over ground between 06:00 and 08:00 UTC. The dissipation phase, started around 09:00 UTC, concluded after about 1 h. Interestingly, the lower left panel of Fig. 9 shows the registered lightnings. The radar observations allow to catch the storm development, especially the northern part, as it can be noticed by Fig. 10 showing some crucial time frames in terms of VMI. At 04:00 UTC a small-sized convective cell is identifiable eastward. After half an hour, the storm reached a pretty mature stage with reflectivity core largely exceeding 50 dBZ. Around 04:50 UTC, the effects of signal extinction become manifest eastward at about 40 km from the radar site. The shielding effect is deeper 10 min later as a consequence of the further storm development. The storm assumes a multi-cellular structure around 05:30 UTC when the southern cell started to hit Siracusa. As it can be noticed by Fig. 11, the approximate Freezing Layer Height (FLH) was located around 3.4 km Above Sea Level (A.S.L.) around 08:00 UTC, according to the radar observations collected at vertical incidence. Figure 11 also shows that Z_{DR} was affected by a relatively negligible bias, being within 0.2 dB. The vertical section of the polararimetric radar measurements is analyzed at 04:50 UTC for the 121st and 122nd azimuthal angles, shown in Figs. 12–14, respectively. Focusing first on the azimuth 121, it is worth noting the reflectivity core located at about 30 km from the radar which extends above 10 km height. High values of Z_{DR} below the presumed freezing layer, noticeable till the reflectivity core, are ascribable to large drops, as also documented by the corresponding correlation coefficient mostly ranging around 0.95. The intrusion of liquid water drops above the FLH is particularly evident through the Z_{DR} column (i.e., vertical distribution of positive Z_{DR} values) in correspondance of the centre of the reflectivity core (Kumjian et al., 2014). The correlated K_{DP} column further testifies the relevant liquid water fraction above the FLH. According to the schematic circulation superimposed to the vertical cut of radial veloc-

CC BY

ity, the strong updraft on the left side of the reflectivity core triggers the supercooling of large drops which turn into hailstones by freezing on condensation nuclei. Beyond the reflectivity core, Z_{DR} is clearly affected by attenuation. More interestingly, the deep depression of ρ_{HV} can be attributed to non-uniform beam filling induced by hail-rain precipitation mixture, as identifed by the adopted hydrometeor classification scheme. In this respect, it is worth specifying that the correlation coeffient is routinely corrected for low SNR through the noise power measured operationally after each volumetric scan. Figure 13 shows the range plots of the radar observables at 5° of antenna elevation for the same azimuth as in Fig. 12. The precipitation peak, located between 29 and 31 km from the radar, is responsible for about 12 dB of absolute attenuation whereas the estimated differential attenuation is about 2 dB. The corresponding relatively high values of K_{DP} are sintomatic of high liquid water fraction. Consequently, the abrupt decrease arised by the correlation coefficient through the precipitation peak where it drops down to about 0.75, even though the reflectivity is clearly higher than the estimated MDZ (SNR is above 12 dB within 35 km), has to be ascribed to the heterogeneity of the hydrometeor population within the radar beam. As it might be expected, the vertical cut taken at the azimuth 122 shows similar characteristics, altough some features look more pronounced. Looking at Fig. 14, three Z_{DR} columns extends above the FLH. With respect to those in Fig. 12 they appears much more smeared. Contextually, specific differential phase exceedes 5° km^{-1} within the K_{DP} column that can be found at 20 km distance. Moreover, such column is within a region in which ρ_{HV} is low. Accordingly, the hydrometeor classification algorithm detects rain/hail misture or just hail in correspondance of the reflectivity core, respectively below and above the FLH. As shown in Fig. 15, the range profiles taken at 5° of antenna elevation highlights a main precipitation peak, generating about 6 dB of attenuation cumulated in about 4 km. The profile of K_{DP} outlines other 2 secondary precipitation peaks accountig for the rest of the retrieved attenuation which sums in total 10 dB. As for azimuth 121, the correlation coefficient remarkably decreases within the convective core dropping up to 0.85. The map of precipitation cumulated in 6 h is shown in Fig. 16 to conclude the

AMTD
8, 7201–7237, 2015

CC BY

storm analysis. The image clearly outlines that most of the precipitation was observed on the south-eastern coast, with a peak around the city of Siracusa at about 60 km from the radar site. The adopted combined rainfall algorithm retrieved fairly well the precipitation pattern despite the peak was underestimated by about 30 %, i.e. 135 mm vs. 186 mm. The overal error analysis summarized in Table 2, shows a remarkable improvement obtained by the approaches employing K_{DP} especially in the presence of rain–hail mix, when compared to the conventional Z–R inversion technique, especially R_C, outperforming both R_Z and R_K.

4 Conclusions

The present manuscript documented the effective monitoring of intense precipitation events in the Mediterranean area by means of an operational X-band dual-polarization weather radar operated in Catania (Sicily, Italy) by the Department of Civil Protection. Two severe hail-bearing storms, occurred in 2013 in South Italy, have been described in terms of the polarimetric radar signatures and estimated rainfall fields. On the 21 February 2013, a winter convective system originated in the Tyrrhenian sea caused the flash-flood of the city of Catania. Due to the optimal radar location, it has been possible to satisfactorily reconstruct the storm characteristics in a satisfactorily way, in spite of known limitation of X-band systems due to attenuation. A few cases of signal extinction, caused by close-range hail core generating significant differential phase shift in very short range path, were documented. However, intense precipitation did not occur above the radar, keeping negligible the influence of radome attenuation. The second storm event, a mesoscale convective system originated by the temperature gradient between sea and land surface, was observed on the 21 August 2013. It lasted about 6 h with a precipitation peak of 186 mm registered in just a couple of hours in Siracusa which, consequently, was flooded. Although the use of K_{DP} can mitigate issues of rain estimation in the presence of hail/rain mixture (Matrosov et al., 2013), analysis of storms dynamics requires the use of the set of dual-polarization measurements

CC BY

that includes reflectivity and differential reflectivity that, at X-band, are attenuated by propagation along precipitation. Absolute and differential attenuation have been compensated through differential phase measurements, properly processed by means of an iterative approach using a short-length moving window enabling to effectively catch the intrinsic small-scale storm characteristics. The comparative analysis of the polarimetric radar observations, by means of some vertical cut of the volumetric observations, enabled to infer the triggering hail formation and precipitation process during the mature phase of the convective system. The applied Fuzzy Logic hydrometeor classification algorithm confirmed the occurrence of rain–hail precipitation mixture, which likely caused the anomalous drop of the correlation coefficient. The precipitation fields were reconstructed fairly well using a combined polarimetric rainfall algorithm based on reflectivity and specific differential phase, which clearly outperformed the conventional Z–R inversion technique.

Acknowledgements. L. Baldini and N. Roberto acknowledge the support of the agreement between CNR-ISAC and DPC for year 2014.

References

Adirosi, E., Baldini, L., Roberto, N., Vulpiani, G., and Russo, F.: Using disdrometer measured raindrop size distributions to establish weather radar algorithms, AIP Conference Proceedings, 1648, 110–128, available at: http://scitation.aip.org/content/aip/proceeding/aipcp/10.1063/1.4912476, 2015. 7208, 7209

Anagnostou, E. N., Anagnostou, M. N., Krajewski, W. F., Kurger, A., and Mirovsky, B. J.: High-resolution rainfall estimation from X-band polarimetric radar measurements, J. Hydrometeorol., 5, 110–128, 2004. 7203

Anagnostou, M. N., Kalogiros, J., Anagnostou, E. N., Tarolli, M., Papadopoulus, A., and Borga, M.: Performance evaluation of high-resolution rainfall estimation by X-band dual-polarization radar for flash flood applications in mountainous basins, J. Hydrol., 394, 4–16, 2010. 7203

AMTD
8, 7201–7237, 2015

Atlas, D. and Ludlam, F. H.: Multi-wavelength radar reflectivity of hailstorms, Q. J. Roy. Meteor. Soc., 87, 523–534, 1961. 7204
Aydin, K., Seliga, T. A., and Bringi, V. N.: Differential radar scattering properties of model rain hail and mixed-phase hydrometeors, Radio Sci., 19, 58–66, 1984. 7204
Aydin, K., Seliga, T. A., and Balaji, V.: Remote sensing of hail with a dual linear polarization radar, J. Clim. Appl. Meteorol., 34, 404–410, 1986. 7204
Bechini, R., Chandrasekar, V., Cremonini, R., and Lim, S.: Radome attenuation at X-band radar operations, in: Proc. 6th European Conf. on Radar in Meteorology and Hydrology: Adv. in Radar Technology, Sibiu, Romania, 6–10 September 2010. 7203
Biron, D.: LAMPINET – lightning detection in Italy, in: Lightning: Principles, Instruments and Applications, edited by: Betz, H. D., Schumann, U. and Laroche, P., Springer Netherlands, Oxford, 141–159, 2009. 7209
Bringi, V. N., Seliga, T. A., and Aydin, K.: Hail detection with a differential reflectivity radar, Science, 225, 1145–1157, 1984. 7204
Bringi, V. N., Chandrasekar, V., Balakrishnan, N., and Zrnić, D. S.: An examination of propagation effects in rainfall on radar measurements at microwave frequencies, J. Atmos. Ocean. Tech., 7, 829–840, 1990. 7208
Bringi, V. N., Keenan, T., and Chandrasekar, V.: Correcting C-band radar reflectivity and differential refelctivity data for rain attenuation: a self-consistent method with constraints, IEEE T. Geosci. Remote, 39, 1906–1915, 2001. 7208
Carey, L. D., Rutledge, S. A., and Ahijevych, D. A.: Correcting propagation effects in C-band polarimetric radar observations of tropical convection using differential propagation phase, J. Appl. Meteorol., 39, 1405–1433, 2000. 7208
Cook, B.: Hail determination by radar analysis, Mon. Weather Rev., 86, 435–438, 1958. 7204
Dolan, B. and Rutledge, S. A.: A theory-based hydrometeor identification algorithm for X-Band polarimetric radars, J. Atmos. Ocean. Tech., 26, 2071–2088, 2009. 7209
Douglas, R. H. and Hitschfeld, W.: Studies of Alberta hailstorms, 1957, Tech. Rep. MW-27, Stormy Weather Group, McGill University, Montreal, Canada, 1958. 7204
Eccles, P. J. and Atlas, D.: A dual-wavelength radar hail detector, J. Appl. Meteorol., 12, 847–854, 1973. 7204
Figueras and Ventura, J., Honore, F., and Tabary, P.: X-band polarimetric weather radar observations of a hailstorm, J. Atmos. Ocean. Tech., 30, 2143–2151, 2013. 7205, 7208

AMTD
8, 7201–7237, 2015

Gorgucci, E., Scarchilli, G., and Chandrasekar, V.: A Procedure to calibrate multiparameter weather radar using properties of the rain medium, IEEE T. Geosci. Remote, 37, 269–276, 1999. 7207

Heinselman, P. L. and Ryzhkov, A. V.: Validation of polarimetric hail detection, Weather Forecast., 21, 839–850, 2006. 7205

Illingworth, A. J., Goddard, J. W. F., and Cherry, S. M.: Polarization radar studies of precipitation development in convective storms, Q. J. Roy. Meteor. Soc., 113, 469–489, 1987. 7205

Knight, C. A. and Knight, N. C.: The falling behaviour of hailstones, J. Atmos. Sci., 7, 672–681, 1970. 7204

Kumjian, M. R., Khain, A. P., Benmoshe, N., Ilotoviz, E., Ryzhkov, A. V., and Phillips, V. T. J.: The anatomy and physics of ZDR columns: investigating a polarimetric radar signature with a spectral bin microphysical model, J. Appl. Meteorol. Clim., 53, 1820–1843, 2014. 7205, 7212

Liu, H. and Chandrasekar, V.: Classification of hydrometeor type based on multiparameter radar measurements: development of a Fuzzy Logic and Neuro Fuzzy systems and in-situ verification, J. Atmos. Ocean. Tech., 17, 140–164, 2000. 7205, 7209

Marshall, J. S. and Palmer, W. M.: The distribution of raindrops with size, J. Meteorol., 5, 165–166, 1948. 7209

Marzano, F. S., Montopoli, M., Picciotti, E., and Vulpiani, G.: Inside volcanic clouds. Remote sensing of ash plumes using microwave weather radars, B. Am. Meteorol. Soc., 94, 1567–1586, 2013. 7206

Mason, B. J.: The Physics of Clouds, Clarendon Press, Oxford, UK, 1971. 7204

Matrosov, S. Y., Kingsmill, D. E., and Martner, B. E.: The utility of X-band polarimetric radar for quantitative estimates of rainfall parameters, J. Hydrometeorol., 6, 248–262, 2005. 7203

Matrosov, S. Y., Cifelli, R., and Gochis, D.: Measurents of heavy convective rainfall in the presence of hail in flood-prone areas using an X-band polarimetric radar, J. Appl. Meteorol. Clim., 52, 395–407, 2013. 7203, 7205, 7214

Rasmussen, R. M. and Heymsfield, A. J.: Melting and shedding of graupel and hail, J. Atmos. Sci., 44, 2754–2763, 1987. 7204

Ryzhkov, A. V., Kumjian, M. R., Ganson, S. M., and Khain, A. P.: Polarimetric radar characteristics of melting hail. Part I: Theoretical simulations using spectral microphysical modeling, J. Appl. Meteorol. Clim., 52, 2849–2870, 2013. 7203

AMTD
8, 7201–7237, 2015
Characterization of Mediterranean hail-bearing storms
G. Vulpiani et al.

CC BY

Schneebeli, M., Sakuragi, J., Biscaro, T., Angelis, C. F., Carvalho da Costa, I., Morales, C., Baldini, L., and Machado, L. A. T.: Polarimetric X-band weather radar measurements in the tropics: radome and rain attenuation correction, Atmos. Meas. Tech., 5, 2183–2199, doi:10.5194/amt-5-2183-2012, 2012. 7203

Seliga, T. A. and Bringi, V. N.: Potential use of radar reflectivity measurements at orthogonal polarizations for measuring precipitation, J. Appl. Meteorol., 15, 69–76, 1976. 7204

Seliga, T. A., Aydin, K., Cato, C. P., and Bringi, V. N.: Use of the differential reflectivity radar technique for observing convective systems, in: Cloud Dynamics, edited by: Agee, M. and Asai, T., Reidel, Dordrecht, the Netherlands, 285–300, 1982. 7204

Smyth, T. J., Blackman, T. M., and Illingworth, A. J.: Observations of oblate hail using dual polarization radar and implications for hail-detection schemes, Q. J. Roy. Meteor. Soc., 125, 993–1016, 1999. 7204

Snyder, J. C., Bluestein, H. B., Zhang, G., and Frasier, S. J.: Attenuation correction and hydrometeor classification of high-resolution, x-band, dual-polarized mobile radar measurements in severe convective storms, J. Atmos. Oceanic Technol., 27, 1979–2001, doi:10.1175/2010JTECHA1356.1, 2010. 7205

Tabary, P., Vulpiani, G., Gourley, J. J., Illingworth, A. J., Thompson, R. J., and Bousquet, O.: Unusually high differential attenuation at C-band: results from a two-year analysis of the French Trappes polarimetric radar data, J. Appl. Meteorol. Clim., 48, 2037–2053, 2009. 7204

Testud, J., Bouar, E. L., Obligis, E., and Ali-Mehenni, M.: The rain profiling algorithm applied to polarimetric weather radar, J. Atmos. Ocean. Tech., 17, 332–356, 2000. 7208

Vivekanandan, J., Yates, D. N., and Brandes, E. A.: The influence of terrain on rainfall estimation from reflectivity and specific propagation phase observations, J. Atmos. Ocean. Tech., 16, 837–845, 1999. 7205

Vulpiani, G. and Baldini, L.: Observations of a severe hail-bearing storm by an operational X-band polarimetric radar in the Mediterranean area, in: Proceed. of the 36th AMS Conference on Radar Meteorology, Breckenridge, CO, USA, 16–20 September 2013. 7208

Vulpiani, G., Montopoli, M., Passeri, L. D., Gioia, A., Giordano, P., and Marzano, F. S.: On the use of dual-polarized C-band radar for operational rainfall retrieval in mountainous areas, J. Appl. Meteorol. Clim., 51, 405–425, 2012. 7206, 7207

Waldvogel, A., Federer, B., and Grimm, P.: Criteria for the detection of hail cells, J. Appl. Meteorol., 18, 167–172, 1979. 7204

Wang, Y. and Chandrasekar, V.: Quantitative precipitation estimation in the CASA X-band dual-polarization radar network, J. Atmos. Ocean. Tech., 27, 1665–1676, 2010. 7203

Zrnić, D. S., Bringi, V. N., Balakrishnan, N., Aydin, K., Chandrasekar, V., and Hubbert, J.: Polarimetric measurements in a severe hailstorm, Mon. Weather Rev., 121, 2223–2238, 1993. 7204

Zrnić, D. S., Ryzhkov, A. V., Straka, J., Liu, Y., and Vivekanandan, J.: Testing a procedure for the automatic classification of hydrometeor types, J. Atmos. Ocean. Tech., 18, 892–913, 2001. 7205

AMTD

8, 7201–7237, 2015

Characterization of Mediterranean hail-bearing storms

G. Vulpiani et al.

Title Page

Abstract | Introduction

Conclusions | References

Tables | Figures

Back | Close

Full Screen / Esc

Printer-friendly Version

Interactive Discussion

Table 1. Error scores computed on hourly cumulated rainfall for the event observed on the 21 February 2013.

Algorithm	$\overline{\varepsilon}$	σ_{ε}	RMSE	FSE	BIAS
R_Z	−1.62	2.12	2.65	0.64	0.61
R_K	−0.36	2.64	2.63	0.64	0.91
R_C	−0.81	2.16	2.28	0.55	0.80

AMTD
8, 7201–7237, 2015
Characterization of Mediterranean hail-bearing storms
G. Vulpiani et al.

Table 2. Error scores computed on hourly cumulated rainfall for the event observed on the 21 August 2013.

Algorithm	$\overline{\varepsilon}$	σ_{ε}	RMSE	FSE	BIAS
R_Z	–2.68	12.41	12.59	1.71	0.63
R_K	0.88	10.44	10.39	1.41	1.12
R_C	–0.62	9.97	9.97	1.36	0.92

AMTD
8, 7201–7237, 2015

CC BY

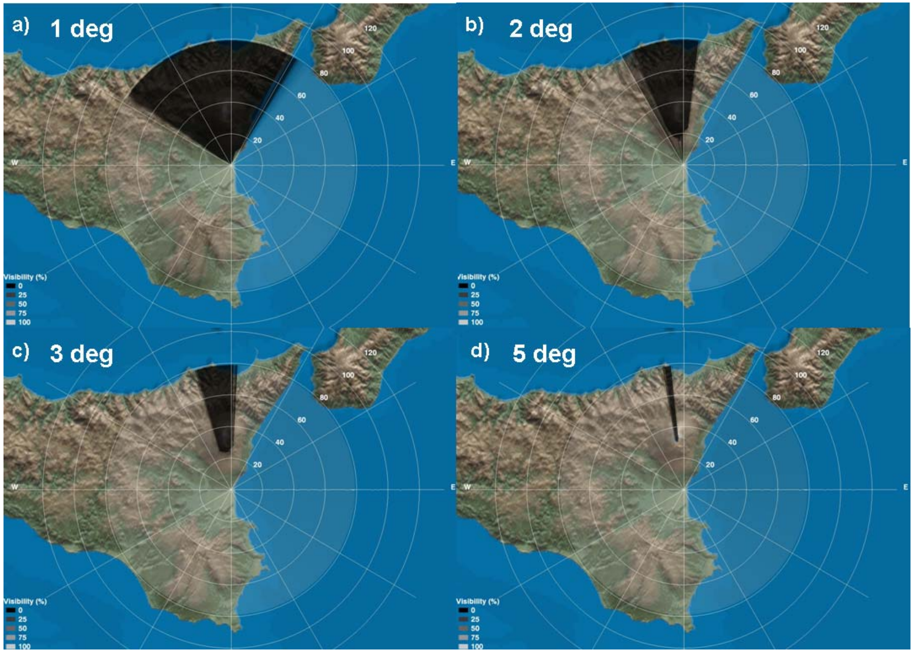

Figure 1. Visibility maps for the considered radar system as retrieved using a 250 m Digital Terrain Model (DTM) at 1, 2, 3 and 5° of antenna elevation.

AMTD
8, 7201–7237, 2015

Characterization of Mediterranean hail-bearing storms

G. Vulpiani et al.

CC BY

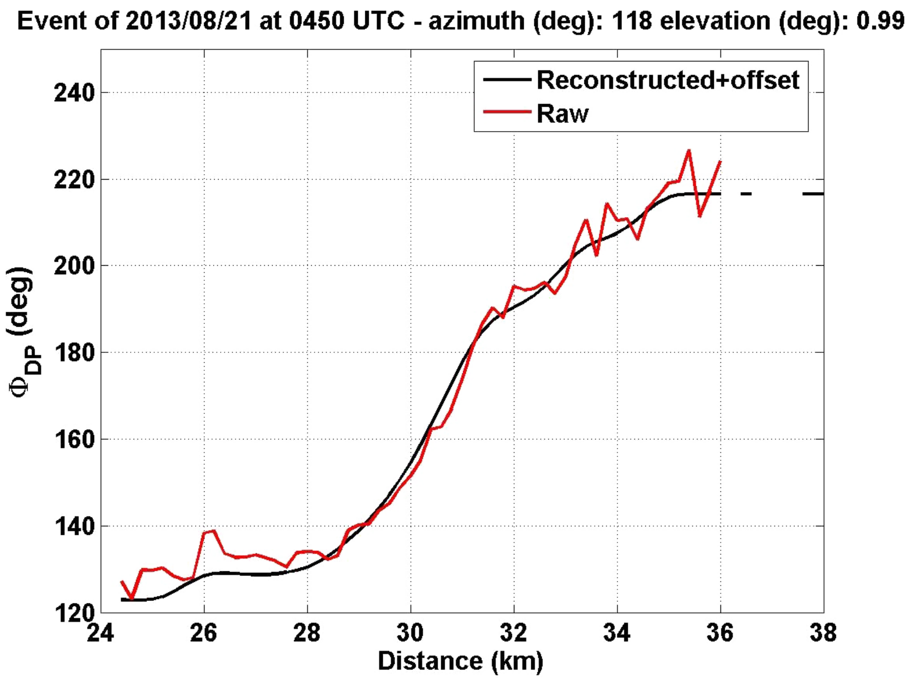

Figure 2. Example of observed and filtered Φ_{DP} range profiles observed on the 21 August 2013 at 04:50 UTC. The estimated offset has been added to the filtered Φ_{DP} to simply the intercomparison.

AMTD
8, 7201–7237, 2015

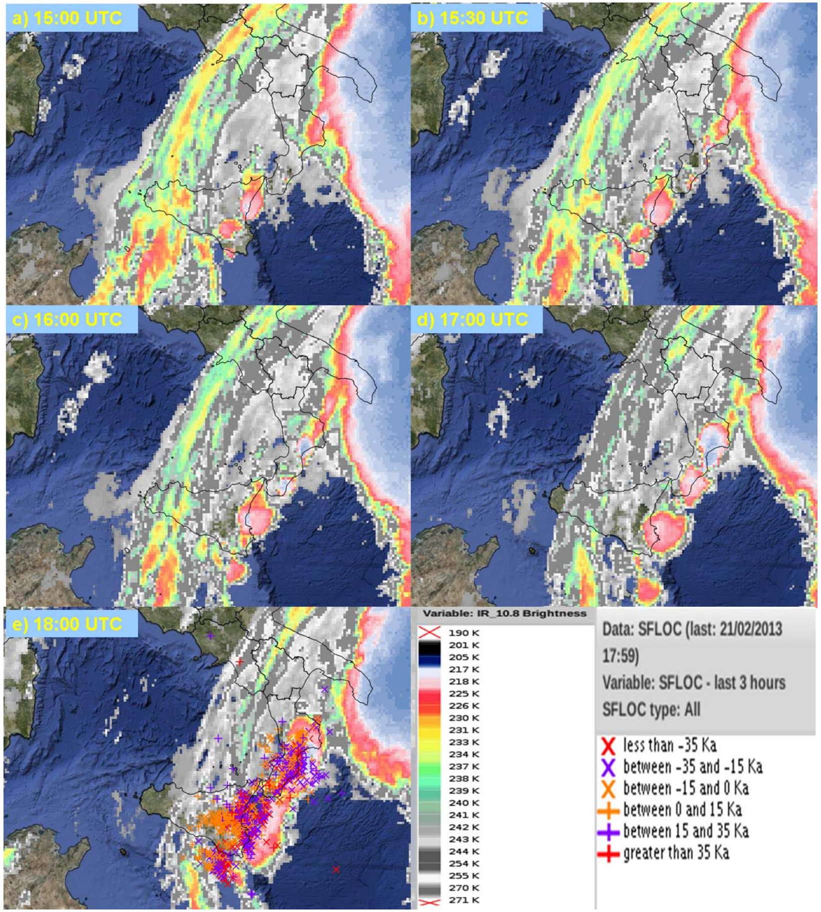

Figure 3. Brightness temperature at 10.8 µm as retrieved on the 21 February 2013 by Spinning Enhanced Visible and Infrared Imager (SEVIRI) instrument on board of the Meteosat Second Generation (MTG) geostationary satellite.

CC BY

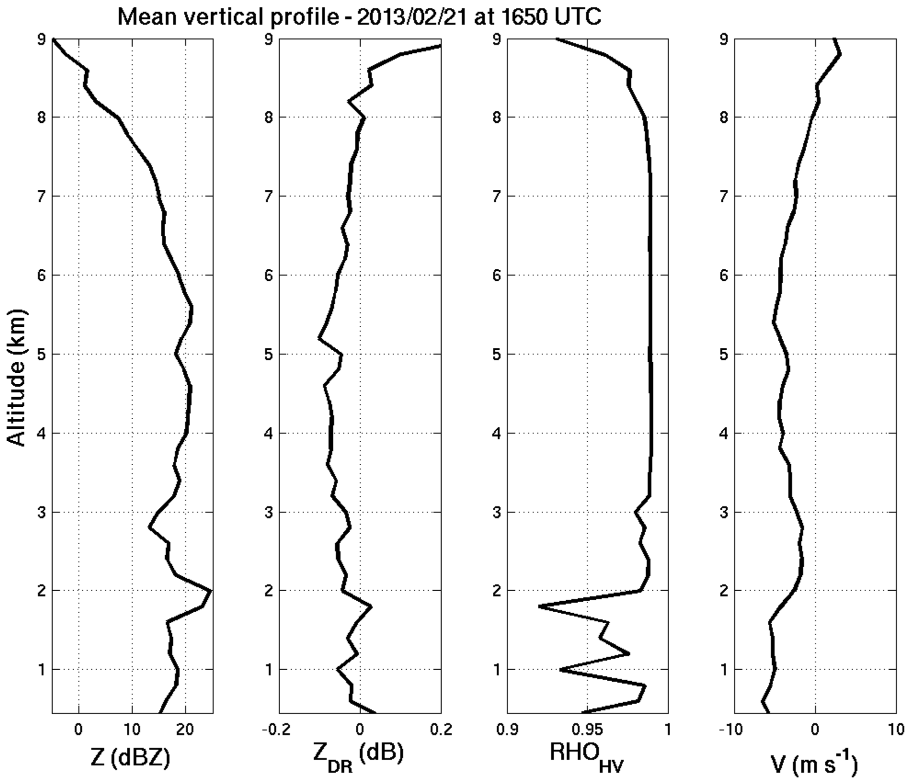

Figure 4. Mean vertical profiles of reflectivity, differential reflectivity, correlation coefficient and Doppler velocity observed on the 21 February 2013 at 16:50 UTC.

AMTD
8, 7201–7237, 2015

Characterization of Mediterranean hail-bearing storms

G. Vulpiani et al.

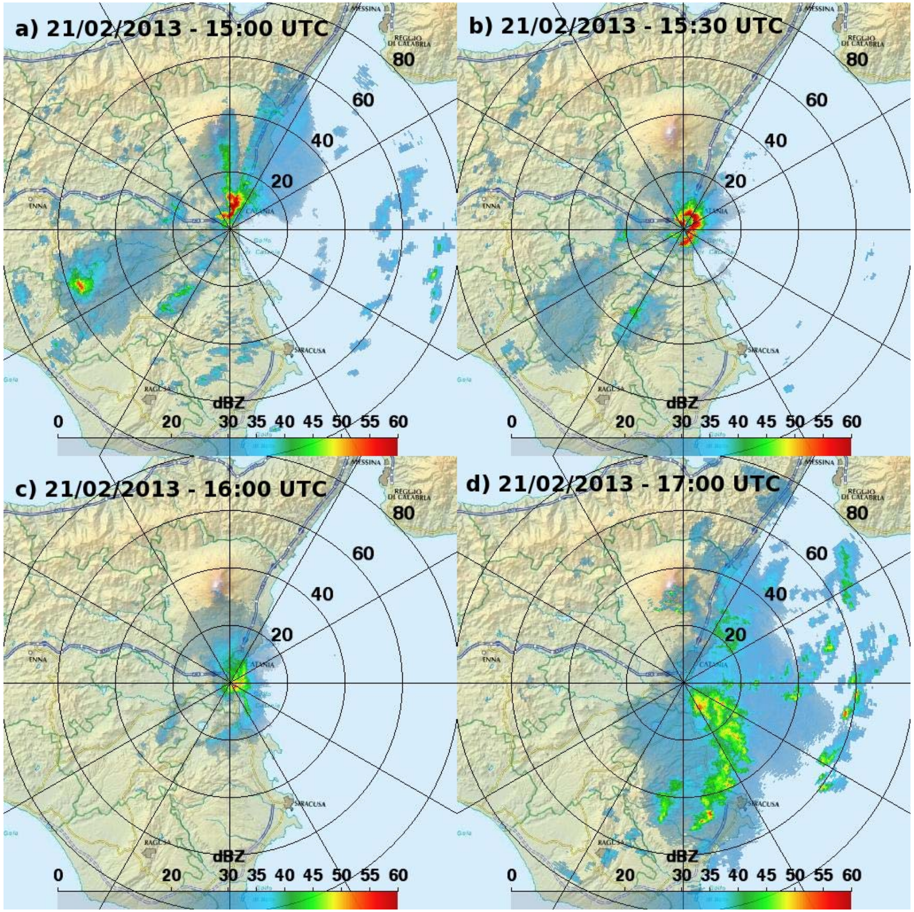

Figure 5. Vertical Maximum Intensity maps as retrieved on the 21 February 2013 at 15:00, 15:30, 16:00 and 17:00 UTC.

AMTD
8, 7201–7237, 2015

Characterization of Mediterranean hail-bearing storms

G. Vulpiani et al.

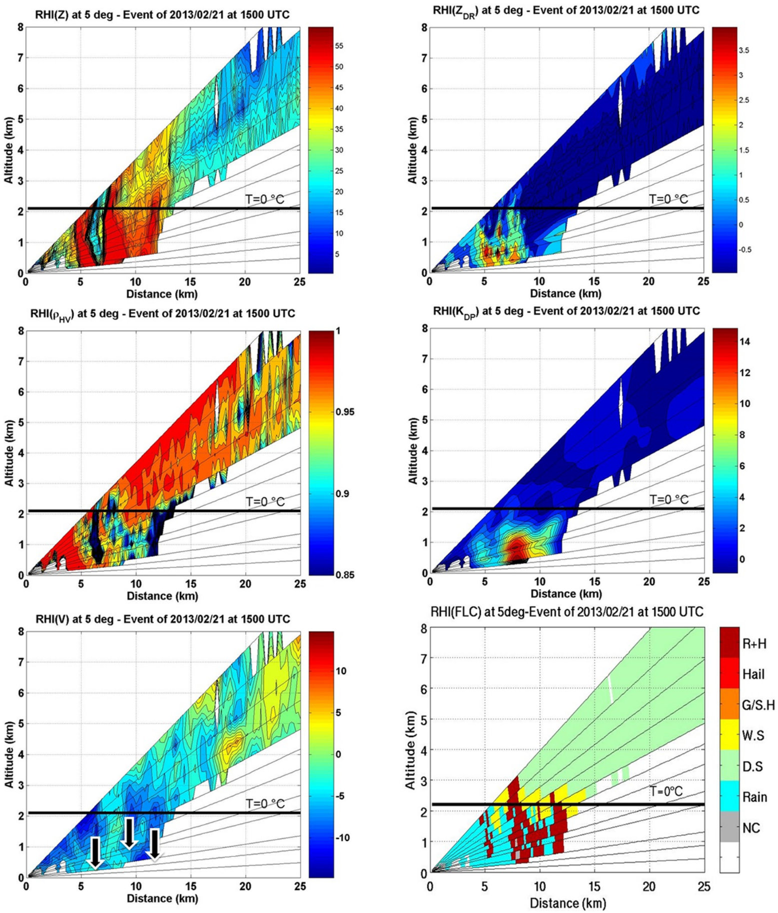

Figure 6. Vertical cut of Z (upper left panel), Z_{DR} (upper right panel), ρ_{HV} (middle left panel), K_{DP} (middle right panel), radial velocity (lower left panel) and hydrometeor classes (lower right panel) taken at 5° of azimuth on the 21 February 2013 at 15:00 UTC.

AMTD
8, 7201–7237, 2015

CC BY

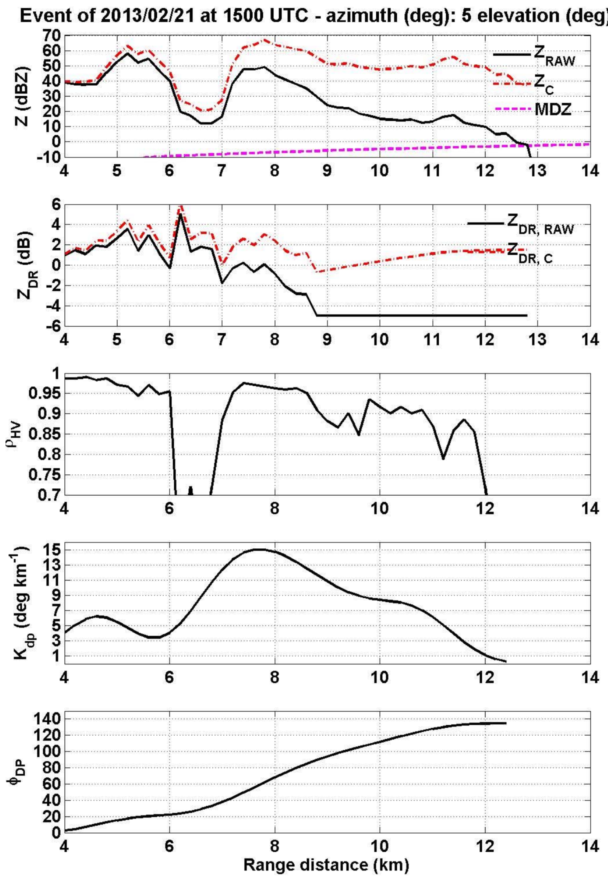

Figure 7. Range plots of the polarimetric radar parameters Z, Z_{DR}, ρ_{HV}, K_{DP} and Φ_{DP} taken at 5° of azimuth and 6° of antenna elevation on the 21 February 2013 at 15:00 UTC. The two upper panels also show the attenuation corrected reflectivity and differential reflectivity. The Minimum Detectable Z (MDZ) is also plotted on the upper panel.

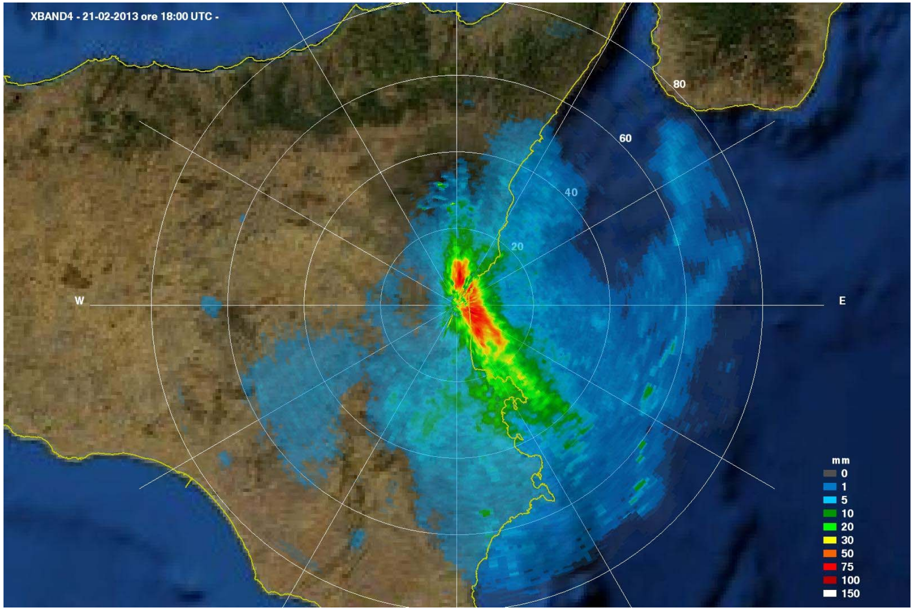

Figure 8. Map of cumulated precipitation as retrieved by the combined polarimetric algorithm between 15:00 and 18:00 UTC on the 21 February 2013.

AMTD
8, 7201–7237, 2015

Characterization of Mediterranean hail-bearing storms

G. Vulpiani et al.

CC BY

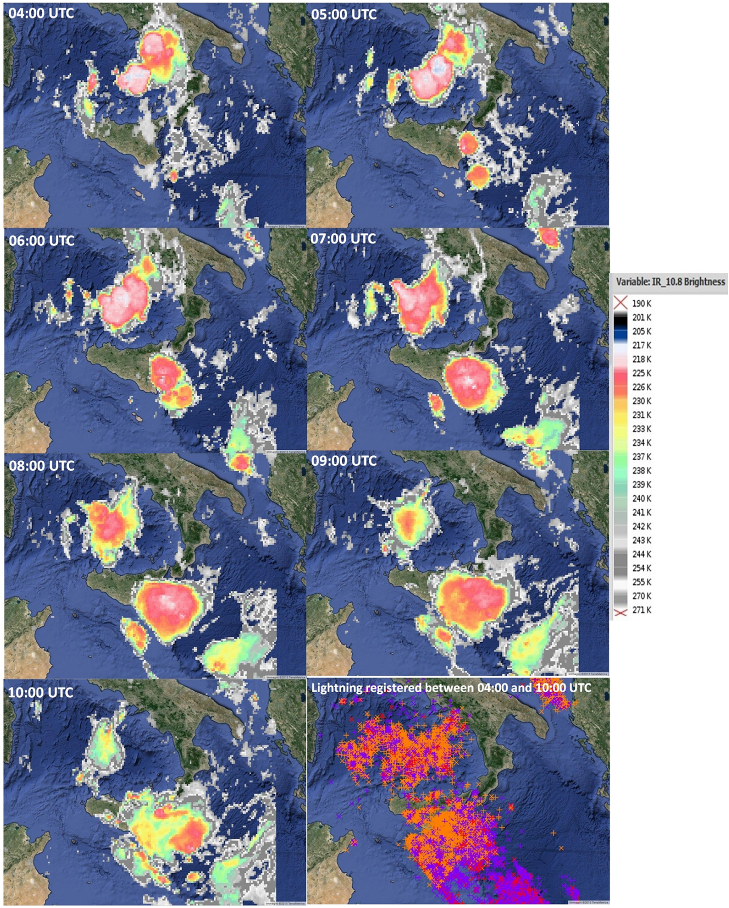

Figure 9. Brightness temperature at 10.8 µm as retrieved on the 21 August 2013 by Spinning Enhanced Visible and Infrared Imager (SEVIRI) instrument on board of the Meteosat Second Generation (MSG) geostationary satellite.

AMTD
8, 7201–7237, 2015

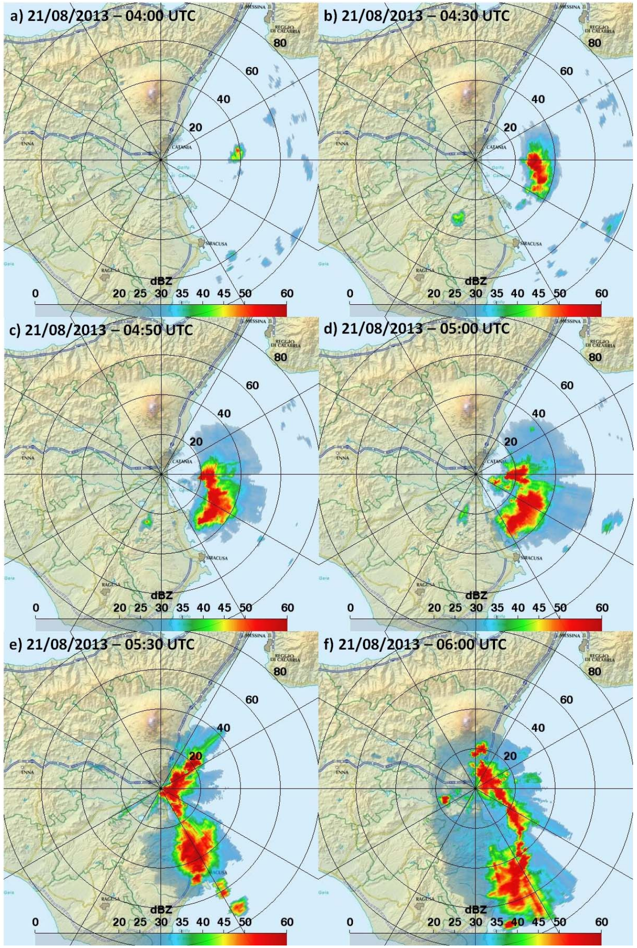

Figure 10. Vertical Maximum Intensity maps as retrieved on the 21 August 2013 at 04:00, 04:30, 04:50, 05:00, 05:30 and 06:00 UTC.

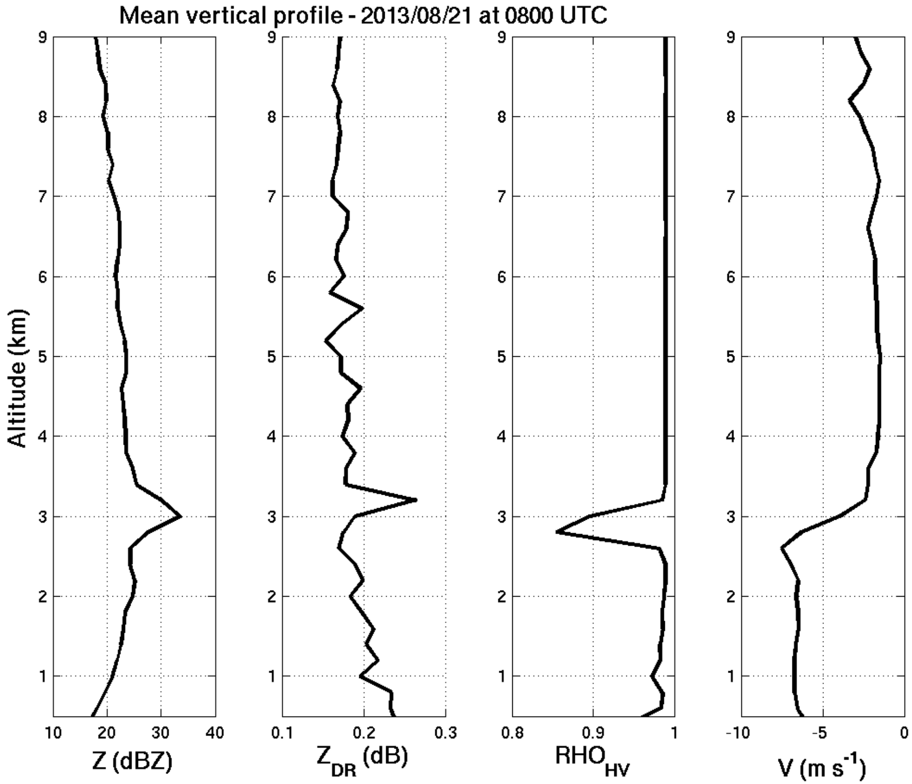

Figure 11. Mean vertical profiles of reflectivity, differential reflectivity, correlation coefficient and Doppler velocity observed on the 21 August 2013 at 08:00 UTC.

AMTD
8, 7201–7237, 2015

Characterization of Mediterranean hail-bearing storms

G. Vulpiani et al.

CC BY

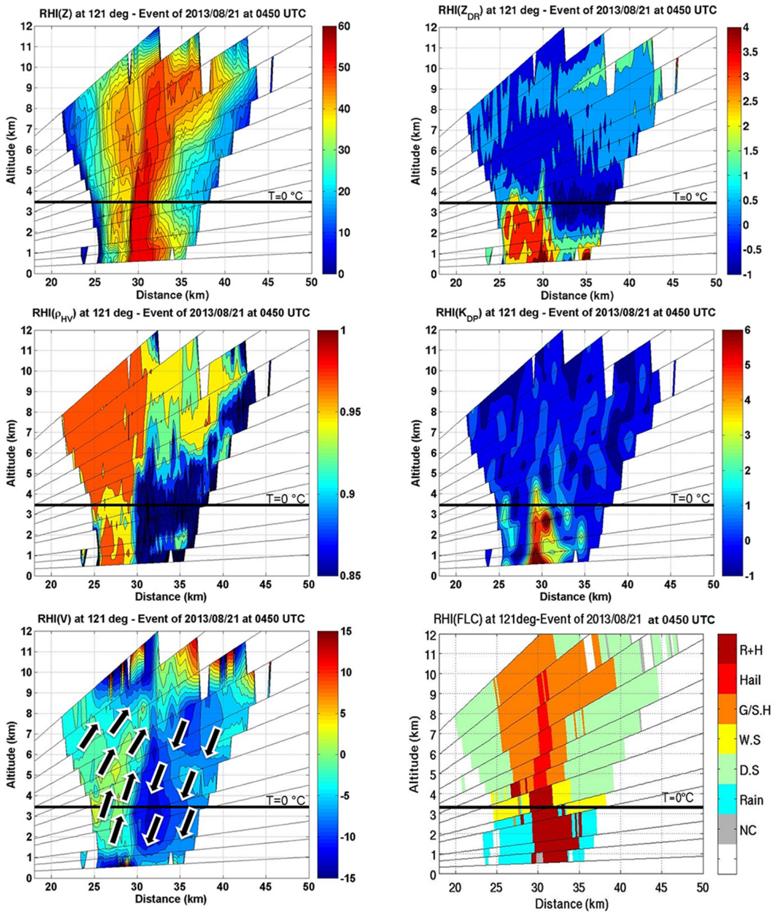

Figure 12. Vertical cut of Z (upper left panel), Z_{DR} (upper right panel), ρ_{HV} (middle left panel), K_{DP} (middle right panel), radial velocity (lower left panel) and hydrometeor classes (lower right panel) taken at 121° of azimuth on the 21 August 2013 at 04:50 UTC.

CC BY

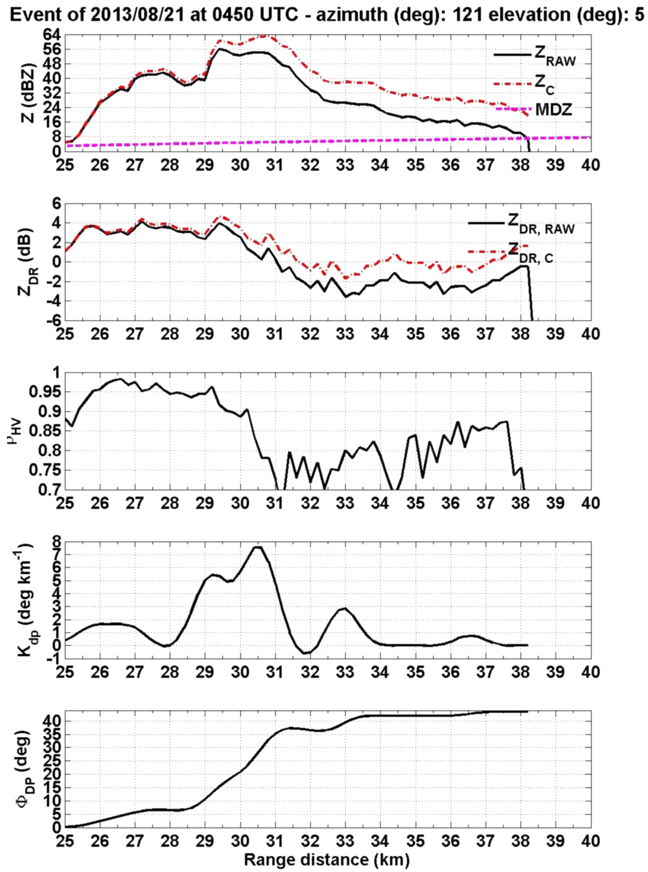

Figure 13. Range plots of the polarimetric radar parameters Z, Z_{DR}, ρ_{HV}, K_{DP} and Φ_{DP} taken at 121° of azimuth and 5° of antenna elevation on the 21 February 2013 at 04:50 UTC. The two upper panels also show the attenuation corrected reflectivity and differential reflectivity. The Minimum Detectable Z (MDZ) is also plotted on the upper panel.

AMTD
8, 7201–7237, 2015

CC BY

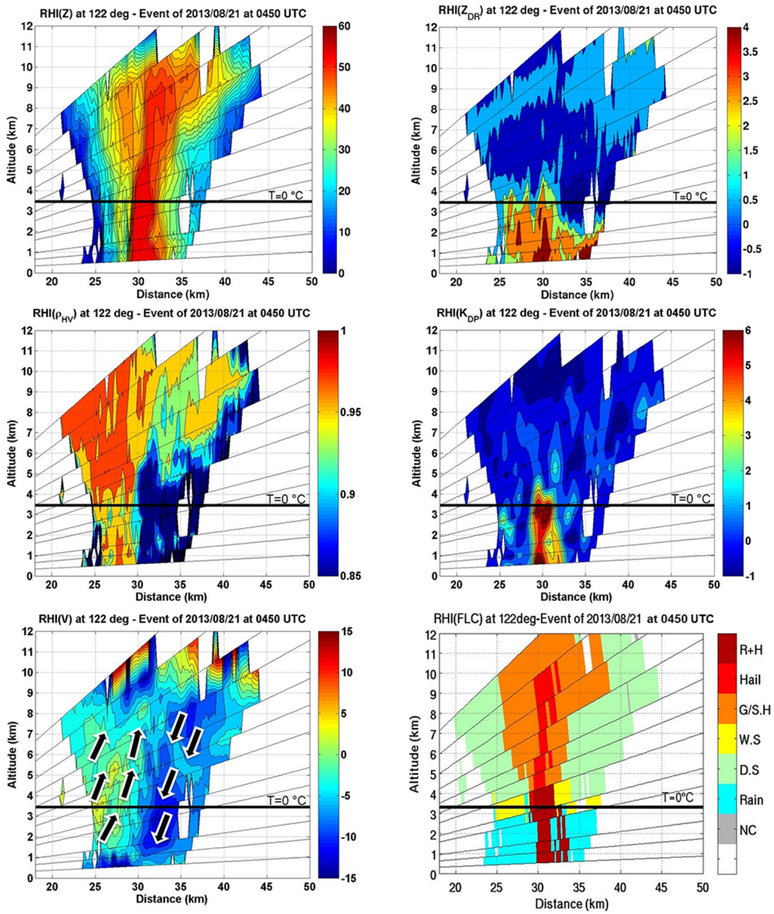

Figure 14. Vertical cut of Z (upper left panel), Z_{DR} (upper right panel), ρ_{HV} (middle left panel), K_{DP} (middle right panel), radial velocity (lower left panel) and hydrometeor classes (lower right panel) taken at 121° of azimuth on the 21 August 2013 at 04:50 UTC.

CC BY

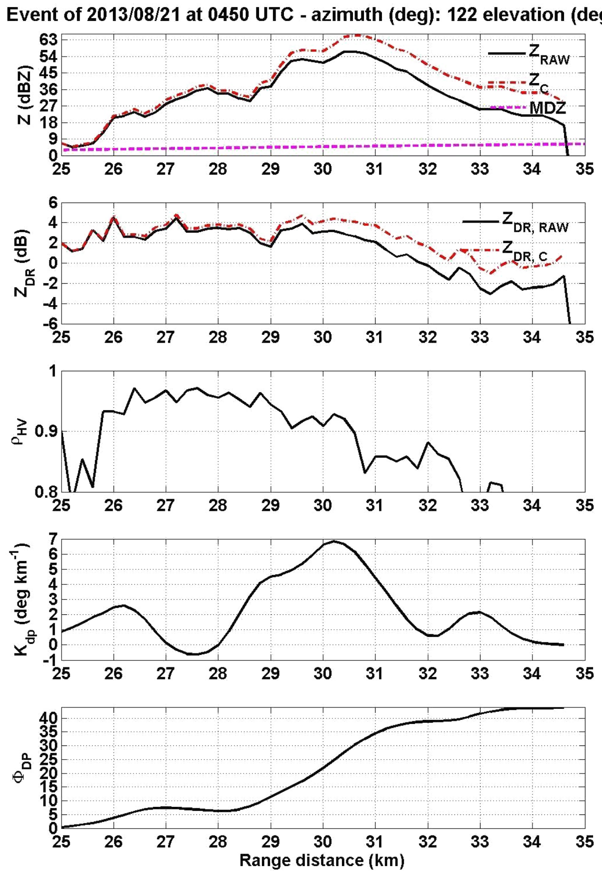

Figure 15. Range plots of the polarimetric radar measurements Z, Z_{DR}, ρ_{HV}, K_{DP} and Φ_{DP} taken at 122° of azimuth and 3° of antenna elevation on the 21 February 2013 at 04:50 UTC. The two upper panels also show the attenuation corrected reflectivity and differential reflectivity. The Minimum Detectable Z (MDZ) is also plotted on the upper panel.

Discussion Paper | Discussion Paper | Discussion Paper | Discussion Paper |

AMTD
8, 7201–7237, 2015
Characterization of Mediterranean hail-bearing storms
G. Vulpiani et al.

CC BY

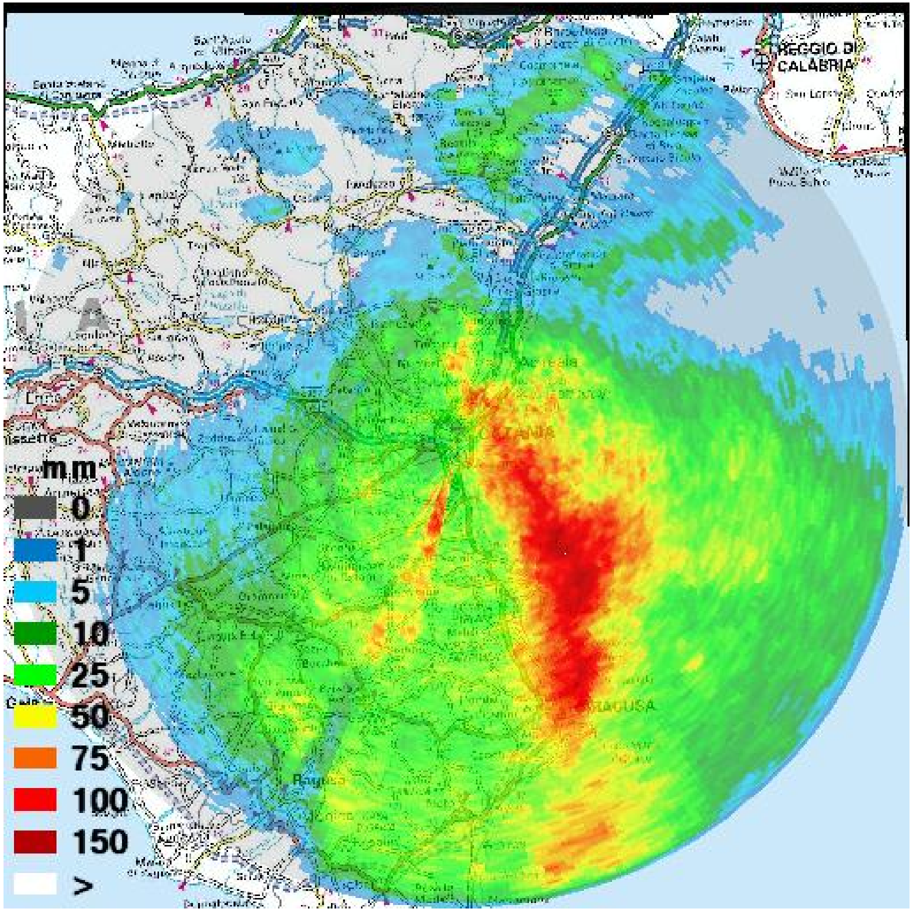

Figure 16. Map of cumulated precipitation as retrieved by the combined polarimetric algorithm between 04:00 and 10:00 UTC on the 21 August 2013.

AMTD
8, 7201–7237, 2015

Characterization of Mediterranean hail-bearing storms

G. Vulpiani et al.

Title Page
Abstract | Introduction
Conclusions | References
Tables | Figures
◂ | ▸
◂ | ▸
Back | Close
Full Screen / Esc
Printer-friendly Version
Interactive Discussion